

Dynamical Polarization of the Fermion Parity in a Nanowire Josephson Junction

J. J. Wesdorp^{1,*}, L. Grünhaupt¹, A. Vaartjes¹, M. Pita-Vidal¹, A. Bargerbos¹, L. J. Splitthoff¹,
P. Krogstrup³, B. van Heck^{2,4,5} and G. de Lange^{2,†}


¹*QuTech and Kavli Institute of Nanoscience, Delft University of Technology, 2628 CJ, Delft, Netherlands*

²*Microsoft Quantum Lab Delft, 2628 CJ, Delft, Netherlands*

³*NNF Quantum Computing Programme, Niels Bohr Institute, University of Copenhagen, Denmark*

⁴*Leiden Institute of Physics, Universiteit Leiden, Niels Bohrweg 2, 2333 CA Leiden, Netherlands*

⁵*Dipartimento di Fisica, Sapienza Università di Roma, P.le Aldo Moro 2, 00185 Roma, Italy*

 (Received 25 January 2022; revised 22 January 2023; accepted 14 July 2023; published 15 September 2023)

Josephson junctions in InAs nanowires proximitized with an Al shell can host gate-tunable Andreev bound states. Depending on the bound state occupation, the fermion parity of the junction can be even or odd. Coherent control of Andreev bound states has recently been achieved within each parity sector, but it is impeded by incoherent parity switches due to excess quasiparticles in the superconducting environment. Here, we show that we can polarize the fermion parity dynamically using microwave pulses by embedding the junction in a superconducting LC resonator. We demonstrate polarization up to $94\% \pm 1\%$ ($89\% \pm 1\%$) for the even (odd) parity as verified by single shot parity readout. Finally, we apply this scheme to probe the flux-dependent transition spectrum of the even or odd parity sector selectively, without any postprocessing or heralding.

DOI: [10.1103/PhysRevLett.131.117001](https://doi.org/10.1103/PhysRevLett.131.117001)

Josephson junctions (JJs) play an essential role in the field of circuit quantum electrodynamics [1], providing the non-linearity required for quantum-limited amplification and quantum information processing [2–5]. Microscopically, the Josephson current is carried by Andreev bound states (ABSs) [6,7]. Recent advances in hybrid circuits with JJs consisting of superconducting atomic break junctions [8–10] or superconductor-semiconductor-superconductor weak links [11–14] have opened up exciting research avenues due to the presence of few, transparent, tunable ABSs.

ABSs are fermionic states occurring in Kramers' degenerate doublets [7]. Their energy depends on the phase difference across the JJ, and the degeneracy can be lifted in the presence of spin-orbit coupling [15] or magnetic field. Each doublet can be occupied by zero or two, or one quasiparticle (QP), giving rise to even and odd parity sectors. Theoretical proposals have investigated both sectors as qubit degrees of freedom [15–18], relying on conservation of fermion parity. These “Andreev qubits” combine the beneficial small size of semiconductor qubits with strong (spin) state-dependent supercurrents allowing fast, high-fidelity, microwave based readout and manipulation similar to superconducting qubits [10,19,20].

A difficulty is that superconducting circuits contain a nonequilibrium population of QPs [21–32], which can enter the junction and “poison” the ABSs on timescales of $\approx 100 \mu\text{s}$ [10,20,33]. Despite this, recent experiments have demonstrated remarkable control over the ABS dynamics using microwave drives. References [10,20] were able to demonstrate coherent manipulation in the even

parity manifold, while Refs. [19,34,35] focused on the odd manifold and coherently controlled a trapped QP and its spin. In both cases poisoning events must be monitored to operate in the intended parity sector.

So far, the strategy to control the ABS parity has been to engineer the free energy landscape via electrostatic [36,37] or flux [33] tuning to make the QP trapping and detrapping equilibrium rates strongly unbalanced. Applications like Andreev qubits [10,15–20,38] or Majorana detection [39] for topological qubits [40] require to dynamically set the parity without changing gate or flux settings, e.g., using a microwave drive. While microwave photons are only allowed to drive transitions that preserve parity, they should be able to polarize the fermion parity of a JJ by exciting one QP into the continuum of states above the superconducting gap in the leads [15,41–44]. However, so far microwaves have only been observed to increase the rate of QP escape [19,45,46] or trapping [47] from the junction, while deterministic polarization toward either parity has not yet been demonstrated.

In this Letter, we demonstrate dynamical polarization of the fermion parity of ABSs in a nanowire JJ using only microwave control. We first demonstrate single shot readout of the ABS parity. We then show that we can polarize the ABSs into either parity depending on the frequency and power of a second pumping tone. Using a two-state rate model, we infer that the pumping tone can change the transition rate from even to odd parity, or vice versa, by more than an order of magnitude. Finally, we show that we can deterministically polarize the ABS parity over a wide

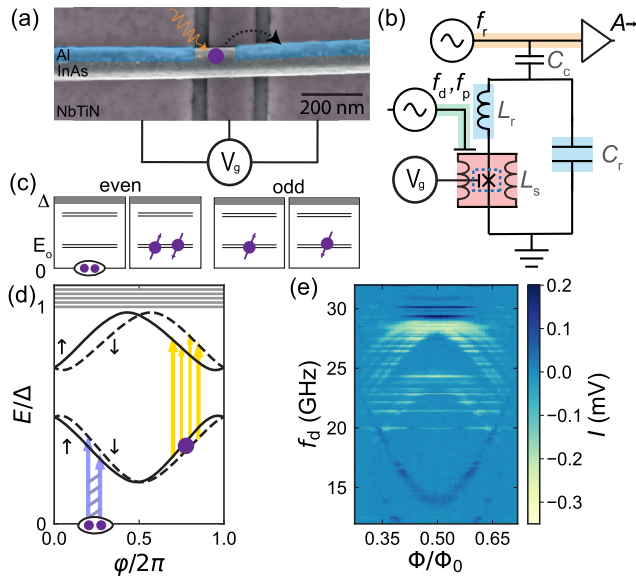


FIG. 1. (a) False-colored scanning electron micrograph of the InAs/Al nanowire JJ formed by etching a ≈ 150 nm section of the Al shell, and sketch of the detrapping of a QP (purple circle) from an ABS by microwave irradiation (yellow arrow). ABSs arise in the semiconducting junction due to constructive interference from consecutive Andreev reflection into the Al leads [20,34,35]. (b) Setup schematic. Two parallel inductances shunt the gate-tunable junction (blue dotted box) and form a gradiometric rf-SQUID (red). For dispersive readout of the ABS spectrum, we integrate the SQUID into an LC resonator (blue) capacitively coupled to a transmission line (orange) and probed with a near-resonant tone at frequency $f_r \approx 4.823$ GHz. A second transmission line (green) allows direct driving of ABS transitions via microwave tones (f_d, f_p). (c) Schematic energy levels of ABSs inside the superconducting gap Δ and the lowest doublet occupation configurations for even and odd junction parity. (d) Energy diagram [34] of levels shown in (c) versus phase bias $\varphi = 2\pi\Phi/\Phi_0$ applied via an external flux Φ . Also indicated are parity-conserving transitions starting from the odd or even parity occupation of the lowest ABS doublet, with colors matching the parity of transitions shown in (e). Blue connected arrows denote transition within the even parity sector starting from the ground state, yellow arrows denote transitions within the odd sector starting with one of the lower levels occupied by a QP. (e) Measured spectrum containing the transitions indicated in (d), starting from odd (yellow) or even (dark blue) parity. Note that spectral copies of the transitions likely are visible due to multiphoton processes involving the cavity photons at $f_d \pm f_r$ [49,63]. Color bar indicates real part (I) of the complex amplitude A of the transmitted tone at f_r [49].

range of flux by pumping at a flux-dependent frequency, as confirmed by parity-selective spectroscopy without post-selection or heralding.

We focus on the microwave transition spectrum of ABSs confined to an InAs nanowire JJ embedded in a radio-frequency superconducting quantum interference device (rf-SQUID) [Fig. 1(a)] [48] acting as a variable series inductance in an LC resonator tank circuit [Fig. 1(b)] [49].

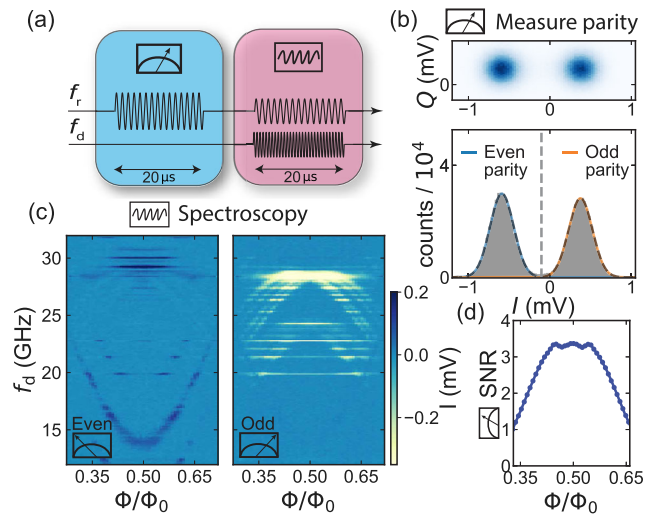


FIG. 2. Spectroscopy conditioned on the result of an initial single shot parity readout. (a) Pulse sequence. We first measure the initial junction parity with a strong $20 \mu\text{s}$ readout pulse at frequency f_r (blue card) and subsequently perform a spectroscopy pulse (red card) consisting of using a weaker $20 \mu\text{s}$ pulse at f_r at the same time as a pulse at variable f_d on the drive line. (b) Top: 2D histogram of rotated parity measurement outcomes at $\Phi = 0.44 \Phi_0$ in the I - Q plane. Bottom: Histogram of the projection to the I axis (gray bars) fitted to a double Gaussian distribution (dashed black line). Blue (orange) lines show single Gaussians using the previously fitted parameters indicating even (odd) initial parity. Dashed gray line indicates the threshold used for parity selection. (c) Postprocessed spectroscopy results of the second pulse conditioned on the initial parity, i.e., the first measurement being left or right from the threshold indicated in (b). Postselection separates the data based on initial parity [cf. Fig. 1(e), where the same data is shown without postprocessing]. (d) Signal to noise ratio (SNR) of the parity measurement.

For driving ABS transitions we include a separate transmission line that induces an ac voltage difference across the junction. The number of ABS levels is controlled by applying a voltage V_g to the bottom gates [60–62]. In order to have a consistent dataset, we keep the gate fixed at $V_g = 0.6248$ V [49].

At this particular V_g , ABS transitions are visible using two-tone spectroscopy [Fig. 1(e)] in the flux range between $0.3\Phi_0$ and $0.7\Phi_0$, where $\Phi_0 = h/2e$. Because of QP poisoning, the parity of the ABSs fluctuates during the measurement [10,20,33]. Thus, the measured spectrum [Fig. 1(e)] is the combination of two sets of transitions with an initial state of either even or odd parity. In Fig. 1(c) we depict a schematic [49] of the relevant ABS levels for this particular V_g . The lowest doublet consists of two spin-dependent fermionic levels (energies $E_o^\uparrow, E_o^\downarrow$) that can either be occupied by a QP or not [64]. The occurrence of odd-parity transitions [yellow lines in Fig. 1(e)] requires the presence of another doublet at higher energies, as generally expected in finite-length weak links or in the presence of multiple transport channels. The ABS levels are spin-split

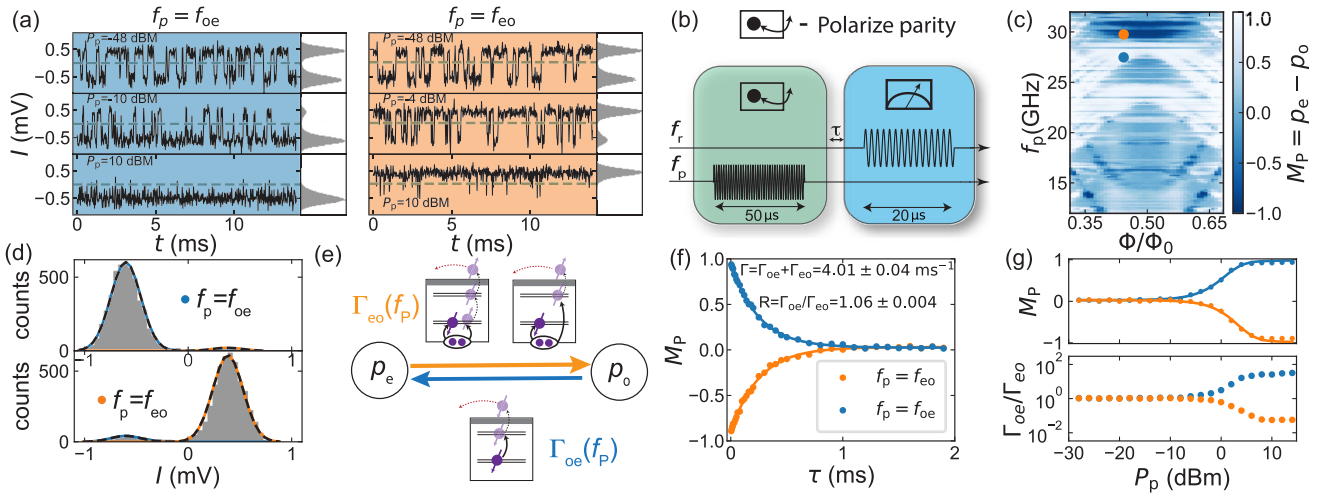


FIG. 3. Dynamical polarization of the junction parity via microwave pumping. (a) Continuous parity monitoring (20 μ s integration time, 15 ms trace), while applying a second tone resonant with one of the odd ($f_{oe} = 27.48$ GHz) or even ($f_{eo} = 29.72$ GHz) parity transitions at low, medium, and strong drive power. Gray histograms show all measured points in the 2 s trace. (b) Pulse scheme used to verify the polarization for panels (c)–(g). A 50 μ s polarization pulse [49] at frequency f_p (green card) is followed after a delay τ by the same parity measurement used in Fig. 2 (blue card). (c) Flux-dependent map of measured parity polarization M_P versus f_p used for the first pulse, where +1 (–1) indicates complete polarization to even (odd) parity. (d) Histograms of I values of the parity measurement after polarization ($P_p = 14$ dBm, $\tau = 4$ μ s) to even (odd) parity via pumping at $f_p = f_{oe}$ ($f_p = f_{eo}$). Flux and f_p set points are indicated by same colored dots in (c). (e) Phenomenological two-state rate model used to describe the parity dynamics and polarization process. Dependent on f_p , either the trapping rate Γ_{eo} or detrapping rate Γ_{oe} increases from its equilibrium value. Sketches of possible processes that increase the rates are shown. Full black arrows indicate the driven transitions, smaller arrows sketch a QP subsequently exiting the junction changing the final state parity and blocking the pumping process. (f) Decay time experiment. First we polarize ($P_p = 14$ dBm) the junction into even (blue dots) or odd (orange dots) parity and then vary τ before the parity measurement. Numbers indicate equilibrium parity switching rates Γ_{oe} , Γ_{eo} extracted from an average of fits (solid lines) of the rate model for different f_p [49]. (g) Pump power dependence of M_P for extracting $R = \Gamma_{oe}/\Gamma_{eo}$ with $\tau = 4$ μ s. Error bars in (f),(g) are smaller than the markers.

at zero field and finite phase drop φ , because spin-orbit coupling induces a spin- and momentum-dependent phase shift gained while traversing the weak link [34,35,38,65], as depicted in Fig. 1(d) [34,49]. Colored arrows indicate transitions visible in Fig. 1(e) with initial odd (yellow) or even (blue) parity.

Without a driving tone, the junction switches between two parity-dependent ground states corresponding to the lowest-energy ABS doublet being empty or occupied by a single QP [66]. We first demonstrate parity readout by doing pulsed spectroscopy conditioned on the outcome of a stronger measurement pulse [Fig. 2(a)] [67]. Readout for both the parity and the spectroscopy pulse is performed with a 20 μ s near-resonant pulse that is short compared to the parity lifetime (~ 0.5 ms) at $f_r \approx 4.823$ GHz that traverses the readout line and interacts with the resonator. From the resulting complex transmitted amplitude $A = I + iQ$ we time-integrate the real (I) and imaginary part (Q). The inductive coupling of the ABSs to the resonator causes a state-dependent dispersive frequency shift of the resonator [10,20,68]. The I , Q values of the parity measurement are thus distributed in two Gaussian sets corresponding to the two parities [Fig. 2(b)]. We fit a double Gaussian distribution to the projection toward the

I axis (black line) from which we extract the even (p_e) and odd (p_o) populations of the ABS [49]. We then postselect the second pulse data conditioned on the measured I in the first pulse being left or right from a Φ -dependent threshold [gray line in Fig. 2(b)] [49]. This allows us to verify that the parity measurement outcomes belong to the even (odd) parity sector by comparing the resulting two-tone spectra of Fig. 2(c) to Fig. 1(e). Finally, we quantify the ability to select on parity by investigating the signal to noise ratio (SNR) of the parity measurement [Fig. 2(d)] [49]. The SNR changes with Φ , reflecting the strong flux dependence of the dispersive shifts of the resonator corresponding to different transitions [68,69].

In the absence of drive, repeated parity measurements yield a near 50-50 split between even and odd [Fig. 2(b)], as reflected by the telegraph noise measured under continuous readout of the cavity at f_r [Fig. 3(a), top]. A second drive tone at a frequency f_p comparable to the ABS transition frequency changes this balance [Fig. 3(a), middle], with the effect increasing at stronger pumping powers P_p [Fig. 3(a), bottom]. In order to rule out a direct effect on the parity readout by the strong drive, we continue with a pulsed experiment [Fig. 3(b)]. We send a pulse at f_p to polarize the parity, followed by a parity measurement (same as in Fig. 2)

on the final state. A delay $\tau = 4 \mu\text{s}$ is inserted between pulses to make sure the resonator is not populated by the polarization pulse. We also expect the delay to allow ABS excitations to decay to their parity-dependent ground state before the readout.

To map out the frequency and flux dependence of the parity polarization, we perform a similar pulse sequence at high P_p versus Φ and f_p [Fig. 3(c)]. We quantify the polarization $M_p = p_e - p_o$ via the parity population imbalance at the end of the sequence. For some f_p the effect is to almost completely suppress one of the two measurements outcomes, indicating that at the end of the pulse the ABSs are initialized in a given parity [Fig. 3(d)]. For instance, at $\Phi = 0.44 \Phi_0$ we reach $M_p = 0.94 \pm 0.01$ for pumping on an odd parity transition ($f_p = 48 \text{ GHz}$) and $M_p = -0.89 \pm 0.01$ for pumping on an even parity transition ($f_p = 29.72 \text{ GHz}$). Note that the resulting parity is opposite to the parity of the pumped transition.

We interpret the polarization to result from the effect of the drive on the parity transition rates. To quantify this, we use a phenomenological model involving two rates Γ_{oe} (for QP detrapping) and Γ_{eo} (for QP trapping) at which the junction switches between even and odd ground states [Fig. 3(e)] [49]. We can estimate Γ_{oe} and Γ_{eo} by varying the delay τ between the drive and measurement pulse at the optimal drive frequencies that initialize the parity [Fig. 3(f)]. In the absence of the drive, two rates are comparable: on average, $R = \Gamma_{oe}/\Gamma_{eo} = 1.06$ and $\Gamma = \Gamma_{oe} + \Gamma_{eo} = 4.01 \pm 0.04 \text{ ms}^{-1}$ [49]. The rates are independent of f_p or P_p used for polarization before the measurement, indicating that when the pump is off, they go back to their equilibrium value on timescales faster than the measurement time and delay used.

To investigate the effect of the drive power on the transition rates, we perform the same pulse sequence as in Fig. 3(b), keeping $\tau = 4 \mu\text{s}$ but varying P_p . From the power dependence of M_p we extract R versus power [Fig. 3(g)], by assuming that we have reached a new steady state at the end of the pump tone [49]. We see that the rates become strongly imbalanced, reaching $R = 32 \pm 9$ ($R^{-1} = 17 \pm 2$) for pumping at f_{oe} (f_{eo}). From Fermi's golden rule, a single photon process would result in a linear increase of the rates with power. However, a phenomenological fit [solid lines in Fig. 3(g)] indicates an exponent larger than one [49]. We therefore suspect multiphoton processes are at play.

The single-photon threshold frequencies expected for trapping and detrapping are $\Delta + \min\{E_o^\uparrow, E_o^\downarrow\}$ and $\Delta - E_o^{\uparrow\downarrow}$ [41–44], respectively, corresponding to the breaking of a pair into one QP in the continuum and one in the ABS, and to the excitation of a trapped QP in the continuum. However, we observe polarization at drive frequencies lower than these thresholds: Γ_{eo} increases already by driving at a frequency $E_o^\uparrow + E_o^\downarrow$, while Γ_{oe} increases when driving resonant with any odd-parity transition [63]. We suspect

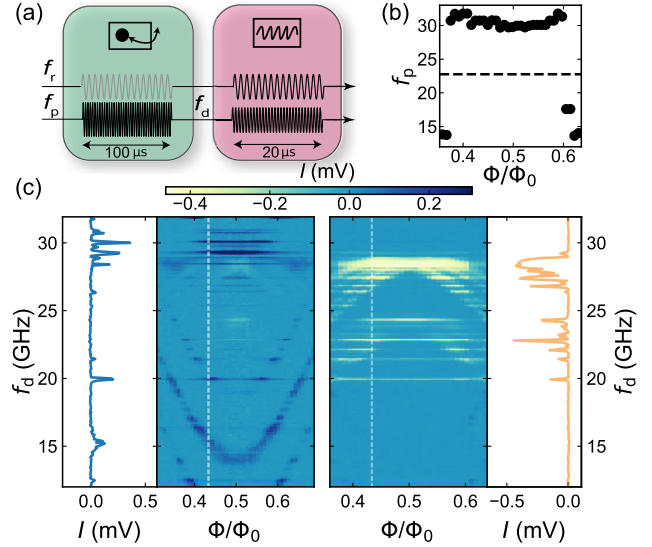


FIG. 4. Deterministic parity initialization verified by spectroscopy for a range of flux values. (a) Pulse sequence. We initialize the parity using a flux-dependent f_p for $100 \mu\text{s}$ together with a low power tone at f_r (green card). This is followed after $5 \mu\text{s}$ by a spectroscopy pulse of $20 \mu\text{s}$ similar to Fig. 2.(a), but without any postselection or heralding (red card). (b) Pump frequency f_p used to increase Γ_{eo} (dots) and Γ_{oe} (dashed line). (c) Result of the second spectroscopy pulse after initializing into even (left panel) or odd parity (right panel). Line cuts at $\Phi = 0.43 \Phi_0$ demonstrate the disappearance of odd (even) transitions after initialization in even (odd) parity.

that the combination of a crowded spectrum—from the multiband-nature of our wire and other modes in the circuit [43]—together with a strong drive allows ladderlike multiphoton processes [sketches in Fig. 3(e)], as suggested in earlier experiments [19,45]. A recent theory work proposed a possible explanation for the parity polarization via a bath-induced coupling of the higher ABS doublet to the continuum [70].

To demonstrate the effectiveness of the parity control, we perform parity-selective two-tone spectroscopy without postselection or heralding. We deterministically initialize the parity of the junction before each spectroscopic measurement via the pumping scheme demonstrated in Fig. 3 followed by a spectroscopy measurement [Fig. 4(a)]. As indicated in Fig. 4(b), at each Φ we adjust the pumping frequency to initialize in the even state to the optimum value experimentally determined in Fig. 3(c), while a constant pumping frequency of 22.76 GHz is adequate to initialize the odd state at all Φ [49]. In Fig. 4(c) the result is shown for even (odd) initialization on the left (right). The similarity with the postselected results of Fig. 2 provides conclusive evidence for the deterministic parity polarization.

In summary, we demonstrated deterministic polarization of the fermion parity in a nanowire Josephson junction using microwave drives. For pumping toward even parity the maximal polarization is limited by parity switches

during the measurement pulse [49]. This mechanism is not sufficient to account for the higher residual infidelity when polarizing to odd parity, which we suspect is due to a finite pumping rate toward the even sector during the polarization pulse. These results enable fast initialization of ABS parity and thus provide a new tool for studying parity switching processes, highly relevant for Andreev [10,19,20] and topological [40] qubits.

Data availability.—Raw data and analysis scripts for all presented figures are available online at Ref. [71].

We thank Ruben Grigoryan for the PCB and enclosure design and Leo Kouwenhoven for support on the project and for commenting on the manuscript. This work is part of the research project “Scalable circuits of Majorana qubits with topological protection” (i39, SCMQ) with project No. 14SCMQ02, which is (partly) financed by the Dutch Research Council (NWO). It has further been supported by the Microsoft Quantum initiative.

*j.j.wesdorp@tudelft.nl

†gijs.delange@microsoft.com

- [1] A. Blais, R.-S. Huang, A. Wallraff, S. M. Girvin, and R. J. Schoelkopf, Cavity quantum electrodynamics for superconducting electrical circuits: An architecture for quantum computation, *Phys. Rev. A* **69**, 062320 (2004).
- [2] M. H. Devoret and R. J. Schoelkopf, Superconducting circuits for quantum information: An outlook, *Science* **339**, 1169 (2013).
- [3] A. Roy and M. Devoret, Introduction to parametric amplification of quantum signals with Josephson circuits, *C.R. Phys.* **17**, 740 (2016).
- [4] G. Wendin, Quantum information processing with superconducting circuits: A review, *Rep. Prog. Phys.* **80**, 106001 (2017).
- [5] M. Kjaergaard, M. E. Schwartz, J. Braumüller, P. Krantz, J. I.-J. Wang, S. Gustavsson, and W. D. Oliver, Superconducting qubits: Current state of play, *Annu. Rev. Condens. Matter Phys.* **11**, 369 (2020).
- [6] I. Kulik, Macroscopic quantization and the proximity effect in S-N-S junctions, *Sov. J. Exp. Theor. Phys.* **30**, 944 (1969), <http://jetp.ras.ru/cgi-bin/e/index/e/30/5/p944?a=list>.
- [7] C. W. J. Beenakker, Universal Limit of Critical-Current Fluctuations in Mesoscopic Josephson Junctions, *Phys. Rev. Lett.* **67**, 3836 (1991).
- [8] L. Bretheau, Ç. Ö. Girit, H. Pothier, D. Esteve, and C. Urbina, Exciting Andreev pairs in a superconducting atomic contact, *Nature (London)* **499**, 312 (2013).
- [9] L. Bretheau, Localized excitations in superconducting atomic contacts: Probing the Andreev doublet, Ph.D. thesis, 2013, https://pastel.hal.science/pastel-00862029/file/Bretheau_Thesis.pdf.
- [10] C. Janvier, L. Tosi, L. Bretheau, Ç. Ö. Girit, M. Stern, P. Bertet, P. Joyez, D. Vion, D. Esteve, M. F. Goffman, H. Pothier, and C. Urbina, Coherent manipulation of Andreev states in superconducting atomic contacts, *Science* **349**, 1199 (2015).
- [11] G. de Lange, B. van Heck, A. Bruno, D. J. van Woerkom, A. Geresdi, S. R. Plissard, E. P. A. M. Bakkers, A. R. Akhmerov, and L. DiCarlo, Realization of Microwave Quantum Circuits Using Hybrid Superconducting-Semiconducting Nanowire Josephson Elements, *Phys. Rev. Lett.* **115**, 127002 (2015).
- [12] T. W. Larsen, K. D. Petersson, F. Kuemmeth, T. S. Jespersen, P. Krogstrup, J. Nygård, and C. M. Marcus, Semiconductor-Nanowire-Based Superconducting Qubit, *Phys. Rev. Lett.* **115**, 127001 (2015).
- [13] L. Casparis, M. R. Connolly, M. Kjaergaard, N. J. Pearson, A. Kringhøj, T. W. Larsen, F. Kuemmeth, T. Wang, C. Thomas, S. Gronin, G. C. Gardner, M. J. Manfra, C. M. Marcus, and K. D. Petersson, Superconducting gatemon qubit based on a proximitized two-dimensional electron gas, *Nat. Nanotechnol.* **13**, 915 (2018).
- [14] M. Pita-Vidal, A. Bargerbos, C.-K. Yang, D. J. van Woerkom, W. Pfaff, N. Haider, P. Krogstrup, L. P. Kouwenhoven, G. de Lange, and A. Kou, A Gate-Tunable, Field-Compatible Fluxonium, *Phys. Rev. Appl.* **14**, 064038 (2020).
- [15] N. M. Chtchelkatchev and Y. V. Nazarov, Andreev Quantum Dots for Spin Manipulation, *Phys. Rev. Lett.* **90**, 226806 (2003).
- [16] A. Zazunov, V. S. Shumeiko, E. N. Bratus', J. Lantz, and G. Wendin, Andreev Level Qubit, *Phys. Rev. Lett.* **90**, 087003 (2003).
- [17] M. A. Desposito and A. Levy Yeyati, Controlled dephasing of Andreev states in superconducting quantum point contacts, *Phys. Rev. B* **64**, 140511(R) (2001).
- [18] C. Padurariu and Y. V. Nazarov, Theoretical proposal for superconducting spin qubits, *Phys. Rev. B* **81**, 144519 (2010).
- [19] M. Hays, V. Fatemi, D. Bouman, J. Cerrillo, S. Diamond, K. Serniak, T. Connolly, P. Krogstrup, J. Nygård, A. L. Yeyati, A. Geresdi, and M. H. Devoret, Coherent manipulation of an Andreev spin qubit, *Science* **373**, 430 (2021).
- [20] M. Hays, G. de Lange, K. Serniak, D. J. van Woerkom, D. Bouman, P. Krogstrup, J. Nygård, A. Geresdi, and M. H. Devoret, Direct Microwave Measurement of Andreev-Bound-State Dynamics in a Proximitized Semiconducting Nanowire, *Phys. Rev. Lett.* **121**, 047001 (2018).
- [21] L. I. Glazman and G. Catelani, Bogoliubov quasiparticles in superconducting qubits, *SciPost Phys. Lecture Notes* **31** (2021), [10.21468/SciPostPhysLectNotes.31](https://doi.org/10.21468/SciPostPhysLectNotes.31)
- [22] J. Aumentado, M. W. Keller, J. M. Martinis, and M. H. Devoret, Nonequilibrium Quasiparticles and $2e$ Periodicity in Single-Cooper-Pair Transistors, *Phys. Rev. Lett.* **92**, 066802 (2004).
- [23] M. Lenander, H. Wang, R. C. Bialczak, E. Lucero, M. Mariantoni, M. Neeley, A. D. O'Connell, D. Sank, M. Weides, J. Wenner, T. Yamamoto, Y. Yin, J. Zhao, A. N. Cleland, and J. M. Martinis, Measurement of energy decay in superconducting qubits from nonequilibrium quasiparticles, *Phys. Rev. B* **84**, 024501 (2011).
- [24] L. Sun, L. DiCarlo, M. D. Reed, G. Catelani, L. S. Bishop, D. I. Schuster, B. R. Johnson, G. A. Yang, L. Frunzio, L. Glazman, M. H. Devoret, and R. J. Schoelkopf, Measurements of Quasiparticle Tunneling Dynamics in a Band-Gap-Engineered Transmon Qubit, *Phys. Rev. Lett.* **108**, 230509 (2012).

- [25] D. Ristè, C. C. Bultink, M. J. Tiggelman, R. N. Schouten, K. W. Lehnert, and L. DiCarlo, Millisecond charge-parity fluctuations and induced decoherence in a superconducting transmon qubit, *Nat. Commun.* **4**, 1913 (2013).
- [26] J. Wenner, Y. Yin, E. Lucero, R. Barends, Y. Chen, B. Chiaro, J. Kelly, M. Lenander, M. Mariantoni, A. Megrant, C. Neill, P. J. J. O'Malley, D. Sank, A. Vainsencher, H. Wang, T. C. White, A. N. Cleland, and J. M. Martinis, Excitation of Superconducting Qubits from Hot Nonequilibrium Quasiparticles, *Phys. Rev. Lett.* **110**, 150502 (2013).
- [27] I. M. Pop, K. Geerlings, G. Catelani, R. J. Schoelkopf, L. I. Glazman, and M. H. Devoret, Coherent suppression of electromagnetic dissipation due to superconducting quasiparticles, *Nature (London)* **508**, 369 (2014).
- [28] U. Vool, I. M. Pop, K. Sliwa, B. Abdo, C. Wang, T. Brecht, Y. Y. Gao, S. Shankar, M. Hatridge, G. Catelani, M. Mirrahimi, L. Frunzio, R. J. Schoelkopf, L. I. Glazman, and M. H. Devoret, Non-Poissonian Quantum Jumps of a Fluxonium Qubit due to Quasiparticle Excitations, *Phys. Rev. Lett.* **113**, 247001 (2014).
- [29] C. Wang, Y. Y. Gao, I. M. Pop, U. Vool, C. Axline, T. Brecht, R. W. Heeres, L. Frunzio, M. H. Devoret, G. Catelani, L. I. Glazman, and R. J. Schoelkopf, Measurement and control of quasiparticle dynamics in a superconducting qubit, *Nat. Commun.* **5**, 5836 (2014).
- [30] R.-P. Riwar, A. Hosseinkhani, L. D. Burkhardt, Y. Y. Gao, R. J. Schoelkopf, L. I. Glazman, and G. Catelani, Normal-metal quasiparticle traps for superconducting qubits, *Phys. Rev. B* **94**, 104516 (2016).
- [31] K. Serniak, M. Hays, G. de Lange, S. Diamond, S. Shankar, L. D. Burkhardt, L. Frunzio, M. Houzet, and M. H. Devoret, Hot Non-Equilibrium Quasiparticles in Transmon Qubits, *Phys. Rev. Lett.* **121**, 157701 (2018).
- [32] W. Uilhoorn, J. G. Kroll, A. Bargerbos, S. D. Nabi, C.-K. Yang, P. Krogstrup, L. P. Kouwenhoven, A. Kou, and G. de Lange, Quasiparticle trapping by orbital effect in a hybrid superconducting-semiconducting circuit, [arXiv:2105.11038](https://arxiv.org/abs/2105.11038).
- [33] M. Zgirski, L. Brethau, Q. Le Masne, H. Pothier, D. Esteve, and C. Urbina, Evidence for Long-Lived Quasiparticles Trapped in Superconducting Point Contacts, *Phys. Rev. Lett.* **106**, 257003 (2011).
- [34] L. Tosi, C. Metzger, M. F. Goffman, C. Urbina, H. Pothier, S. Park, A. L. Yeyati, J. Nygård, and P. Krogstrup, Spin-Orbit Splitting of Andreev States Revealed by Microwave Spectroscopy, *Phys. Rev. X* **9**, 011010 (2019).
- [35] M. Hays, V. Fatemi, K. Serniak, D. Bouman, S. Diamond, G. de Lange, P. Krogstrup, J. Nygård, A. Geresdi, and M. H. Devoret, Continuous monitoring of a trapped, superconducting spin, *Nat. Phys.* **16**, 1103 (2020).
- [36] J. A. van Dam, Y. V. Nazarov, E. P. A. M. Bakkers, S. De Franceschi, and L. P. Kouwenhoven, Supercurrent reversal in quantum dots, *Nature (London)* **442**, 667 (2006).
- [37] S. De Franceschi, L. Kouwenhoven, C. Schönenberger, and W. Wernsdorfer, Hybrid superconductor-quantum dot devices, *Nat. Nanotechnol.* **5**, 703 (2010).
- [38] S. Park and A. L. Yeyati, Andreev spin qubits in multi-channel Rashba nanowires, *Phys. Rev. B* **96**, 125416 (2017).
- [39] E. Prada, P. San-Jose, M. W. A. de Moor, A. Geresdi, E. J. H. Lee, J. Klinovaja, D. Loss, J. Nygård, R. Aguado, and L. P. Kouwenhoven, From Andreev to Majorana bound states in hybrid superconductor-semiconductor nanowires, *Nat. Rev. Phys.* **2**, 575 (2020).
- [40] T. Karzig, C. Knapp, R. M. Lutchyn, P. Bonderson, M. B. Hastings, C. Nayak, J. Alicea, K. Flensberg, S. Plugge, Y. Oreg, C. M. Marcus, and M. H. Freedman, Scalable designs for quasiparticle-poisoning-protected topological quantum computation with Majorana zero modes, *Phys. Rev. B* **95**, 235305 (2017).
- [41] R. P. Riwar, M. Houzet, J. S. Meyer, and Y. V. Nazarov, Shooting quasiparticles from Andreev bound states in a superconducting constriction, *J. Exp. Theor. Phys.* **119**, 1028 (2014).
- [42] R. L. Klees, G. Rastelli, and W. Belzig, Nonequilibrium Andreev bound states population in short superconducting junctions coupled to a resonator, *Phys. Rev. B* **96**, 144510 (2017).
- [43] D. G. Olivares, A. L. Yeyati, L. Brethau, Ç. Ö. Girit, H. Pothier, and C. Urbina, Dynamics of quasiparticle trapping in Andreev levels, *Phys. Rev. B* **89**, 104504 (2014).
- [44] R.-P. Riwar, M. Houzet, J. S. Meyer, and Y. V. Nazarov, Control of Andreev bound state population and related charge-imbalance effect, *J. Phys. Condens. Matter.* **27**, 095701 (2015).
- [45] E. M. Levenson-Falk, F. Kos, R. Vijay, L. Glazman, and I. Siddiqi, Single-Quasiparticle Trapping in Aluminum Nanobridge Josephson Junctions, *Phys. Rev. Lett.* **112**, 047002 (2014).
- [46] J. T. Farmer, A. Zarassi, D. M. Hartsell, E. Vlachos, H. Zhang, and E. M. Levenson-Falk, Continuous real-time detection of quasiparticle trapping in aluminum nanobridge Josephson junctions, *Appl. Phys. Lett.* **119**, 122601 (2021).
- [47] L. Brethau, Ç. Ö. Girit, C. Urbina, D. Esteve, and H. Pothier, Supercurrent Spectroscopy of Andreev States, *Phys. Rev. X* **3**, 041034 (2013).
- [48] J. Clarke and A. I. Braginski, eds., *The SQUID Handbook: Fundamentals and Technology of SQUIDS and SQUID Systems*, 1st ed. (Wiley, New York, 2004).
- [49] See Supplemental Material at <http://link.aps.org/supplemental/10.1103/PhysRevLett.131.117001> for author contributions, circuit fabrication and design details, methods, additional information on the data analysis, a comparison of measured spectra to long junction theory, a description of the rate equations used and related data, a characterization of the parity readout, and additional data on the rates extracted using a continuous readout tone, which includes Refs. [50–59].
- [50] W. Chang, S. M. Albrecht, T. S. Jespersen, F. Kuemmeth, P. Krogstrup, J. Nygård, and C. M. Marcus, Hard gap in epitaxial semiconductor-superconductor nanowires, *Nat. Nanotechnol.* **10**, 232 (2015).
- [51] X. Mi, J. V. Cady, D. M. Zajac, J. Stehlik, L. F. Edge, and J. R. Petta, Circuit quantum electrodynamics architecture for gate-defined quantum dots in silicon, *Appl. Phys. Lett.* **110**, 043502 (2017).
- [52] J. G. Kroll, F. Borsoi, K. L. van der Enden, W. Uilhoorn, D. de Jong, M. Quintero-Pérez, D. J. van Woerkom, A. Bruno, S. R. Plissard, D. Car, E. P. A. M. Bakkers, M. C. Cassidy, and L. P. Kouwenhoven, Magnetic Field Resilient Superconducting Coplanar Waveguide Resonators for Hybrid cQED Experiments, *Phys. Rev. Appl.* **11**, 064053 (2019).

- [53] M. S. Khalil, M. J. A. Stoutimore, F. C. Wellstood, and K. D. Osborn, An analysis method for asymmetric resonator transmission applied to superconducting devices, *J. Appl. Phys.* **111**, 054510 (2012).
- [54] A. Bruno, G. de Lange, S. Asaad, K. L. van der Enden, N. K. Langford, and L. DiCarlo, Reducing intrinsic loss in superconducting resonators by surface treatment and deep etching of silicon substrates, *Appl. Phys. Lett.* **106**, 182601 (2015).
- [55] J. J. Wesdorp, F. J. Matute-Cañadas, A. Vaartjes, L. Grünhaupt, T. Laeven, S. Roelofs, L. J. Splitthoff, M. Pita-Vidal, A. Bargerbos, D. J. van Woerkom, P. Krogstrup, L. P. Kouwenhoven, C. K. Andersen, A. Levy Yeyati, B. van Heck, and G. de Lange, Microwave spectroscopy of interacting Andreev spins, [arXiv:2208.11198](https://arxiv.org/abs/2208.11198).
- [56] D. de Jong, J. van Veen, L. Binci, A. Singh, P. Krogstrup, L. P. Kouwenhoven, W. Pfaff, and J. D. Watson, Rapid Detection of Coherent Tunneling in an InAs Nanowire Quantum Dot through Dispersive Gate Sensing, *Phys. Rev. Appl.* **11**, 044061 (2019).
- [57] S. Machlup, Noise in semiconductors: Spectrum of a two-parameter random signal, *J. Appl. Phys.* **25**, 341 (1954).
- [58] U. Vool, I. M. Pop, K. Sliwa, B. Abdo, C. Wang, T. Brecht, Y. Y. Gao, S. Shankar, M. Hatridge, G. Catelani, M. Mirrahimi, L. Frunzio, R. J. Schoelkopf, L. I. Glazman, and M. H. Devoret, Non-Poissonian Quantum Jumps of a Fluxonium Qubit due to Quasiparticle Excitations, *Phys. Rev. Lett.* **113**, 247001 (2014).
- [59] M. S. Bartlett, Smoothing periodograms from time-series with continuous spectra, *Nature (London)* **161**, 686 (1948).
- [60] Y.-J. Doh, Tunable supercurrent through semiconductor nanowires, *Science* **309**, 272 (2005).
- [61] D. J. van Woerkom, A. Proutski, B. van Heck, D. Bouman, J. I. Väyrynen, L. I. Glazman, P. Krogstrup, J. Nygård, L. P. Kouwenhoven, and A. Geresdi, Microwave spectroscopy of spinful Andreev bound states in ballistic semiconductor Josephson junctions, *Nat. Phys.* **13**, 876 (2017).
- [62] M. F. Goffman, C. Urbina, H. Pothier, J. Nygård, C. M. Marcus, and P. Krogstrup, Conduction channels of an InAs-Al nanowire Josephson weak link, *New J. Phys.* **19**, 092002 (2017).
- [63] Note that we also see peaks in the polarization at transitions $f_{\text{even,odd}} \pm f_r$ due to multiphoton processes involving the cavity. This could be explained by the fact that a weak readout tone was on during the pumping for Fig. 3(c) [49]. Additionally, the copy of the odd-parity transition bundle (also visible in Fig. 2) could be due to the presence of a third ABS doublet in the junction.
- [64] B. van Heck, J. I. Väyrynen, and L. I. Glazman, Zeeman and spin-orbit effects in the Andreev spectra of nanowire junctions, *Phys. Rev. B* **96**, 075404 (2017).
- [65] M. Governale and U. Zülicke, Spin accumulation in quantum wires with strong Rashba spin-orbit coupling, *Phys. Rev. B* **66**, 073311 (2002).
- [66] Configurations with one or more QPs trapped in higher ABS doublets are also possible, to which our parity readout is not sensitive. However, when QPs are trapped in these configurations, they presumably relax to their parity-dependent ground state on timescales much faster than the measured switching time of ~ 0.5 ms that we report in Fig. 3(f). This is supported by recent works on similar nanowires [20,35], which reported 13 μ s for the even excited state, or 3 μ s for the odd excited state.
- [67] For clarity, in Fig. 2(a) we indicate each pulse combination with a colored card and a symbol representing the type of operation, so it can be easily compared with the pulse sequences of Figs. 3(b) and 4(a).
- [68] C. Metzger, S. Park, L. Tosi, C. Janvier, A. A. Reynoso, M. F. Goffman, C. Urbina, A. Levy Yeyati, and H. Pothier, Circuit-QED with phase-biased Josephson weak links, *Phys. Rev. Res.* **3**, 013036 (2021).
- [69] C. Janvier, Coherent manipulation of Andreev bound states in an atomic contact, Ph.D. thesis, Université Paris-Saclay, 2016.
- [70] N. Ackermann, A. Zazunov, S. Park, R. Egger, and A. L. Yeyati, Dynamical parity selection in superconducting weak links, *Phys. Rev. B* **107**, 214515 (2023).
- [71] J. J. Wesdorp, L. Grünhaupt, A. Vaartjes, M. Pita-Vidal, A. Bargerbos, L. J. Splitthoff, P. Krogstrup, B. van Heck, and G. de Lange, Data repository for: Dynamical Polarization of the Fermion Parity in a Nanowire Josephson Junction (2022), 10.4121/17876240.v1.